Structural Engineering and Mechanics, *Vol. 74, No. 3 (2020) 325-339*
DOI: https://doi.org/10.12989/sem.2020.74.3.325

New form of perforated steel plate shear wall in simple frames using topology optimization

Mohammad Hadi Bagherinejad[a] and Abbas Haghollahi*

Faculty of Civil Engineering, Shahid Rajaee Teacher Training University, Tehran, Iran

(Received January 18, 2019, Revised May 4, 2019, Accepted August 27, 2019)

Abstract. This study presents a practical application of topology optimization (TO) technique to seek the best form of perforated steel plate shear walls (PSPSW) in simple frames. For the numerical investigation, a finite element model is proposed based on the recent particular form of PSPSW that is called the ring-shaped steel plate shear wall. The TO is applied based on the sensitivity analysis to maximize the reaction forces as the objective function considering the fracture tendency. For this purpose, TO is conducted under a monotonic and cyclic loading considering the nonlinear behavior (material and geometry) and buckling. Also, the effect of plate thickness is studied on the TO results. The final material volume of the optimized plate is limited to the material volume of the ring-shaped plate. Finally, an optimized plate is introduced and its nonlinear behavior is investigated under a cyclic and monotonic loading. For a more comprehensive view, the results are compared to the ring-shaped and four usual forms of SPSWs. The material volume of the plate for all the models is the same. The results indicate the strength, load-carrying, and energy dissipation in the optimized plate are increased while the fracture tendency is reduced without changing the material volume.

Keywords: topology optimization; perforated steel plate shear walls; simple frame; cyclic loading; sensitivity analysis

1. Introduction

Steel plate shear walls (SPSW) have been rapidly expanded around the world as a lateral resistance system in the last three decades and have been used to construct and retrofit the important building structures, especially in the seismic countries such as Japan and the United States. An SPSW is formed from a steel plate surrounded by the beams and columns, which are referred to as the boundary elements. An SPSW is similar to a cantilever beam in which the columns are the flanges of the beam, the beams of each story are its stiffeners, and the steel plate is the web of beam. The post-buckling strength effect of a steel panel is the basic idea of SPSWs that has been seriously considered in the recent years. In fact, the stiffness of an SPSW is due to the strength of the web plate acting in tension field that is created by the post-buckling mechanism. This mechanism increases the energy dissipation and ductility (Elgaaly 1998, Roberts and Ghomi 1998) but, the post-buckling phenomenon in the SPSW heightens the pinching behavior in the hysteresis behavior (Berman and Bruneau 2005). The pinching behavior of SPSWs in moment frames is mitigated by the moment connections. In simple frames, the pinching behavior of plates appears completely (Vatansever and Yardimci 2011, Valizadeh *et al.* 2012, Shekastehband *et al.* 2017). The pinching behavior caused the U.S. building code allows the use of SPSWs only with the moment frames.

Perforated steel plate shear walls (PSPSW) are required because of architecture reasons or for passing the equipment. On the other hand, the ductility is increased in the PSPSWs. There are several experimental and numerical studies about the performance of PSPSWs that investigated the effects of arrangement and diameter of holes on the behavior of PSPSWs. (Vian *et al.* 2009, Chan *et al.* 2011, Bhowmick *et al.* 2014, Formisano *et al.* 2016, Matteis *et al.* 2016, Kiani and Tsavdaridis 2018). In the usual types of PSPSW, the hole has a circular-shaped and the plate has a central hole or multi holes. Recently Egorova *et al.* (2014) presented a particular form of PSPSW that is called the ring-shaped steel plate shear wall (RS-SPSW). They tested their proposed model in a simple frame with thick plates. RS-SPSW improves the pinching behavior of PSPSW through the mechanism of deforming a circular ring into an ellipse (see Fig.1). They proved that in simple frames, thin infill plates aren't desirable and RS-SPSW with thick plate has a better performance. The use of RS-SPSWs is reasonable in the hazard seismic zones, although its fabrication process is difficult and costly.

By investigating the conducted studies, it is observed that all proposed forms are based on the obtained experiences from the experimental and numerical results. So, the use of an effective method to find the optimized form of the perforated plate is required. Topology optimization (TO) is a powerful tool for providing innovative and optimal engineering designs. The use of TO has been increased with the development and growth of computer science. Gradual progress was made in TO through extensive studies. Introducing different solution methods (Kaveh *et al.* 2008, Gholizadeh and Barati 2014, Khatibinia and Khosravi 2014, Roodsarabi *et al.* 2016,

---

*Corresponding author, Ph.D., Assistant Professor
E-mail: haghollahi@sru.ac.ir
[a] Ph.D. Candidate
E-mail: mh.bagherinejad@sru.ac.ir

http://www.techno-press.com/journals/sem&subpage=7

ISSN: 1225-4568 (Print), 1598-6217 (Online)

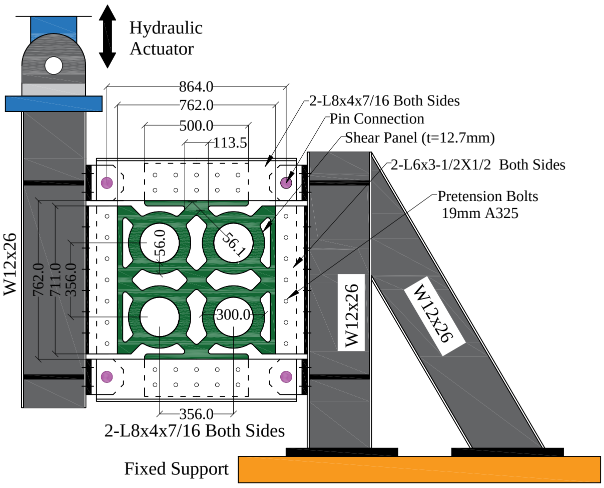

Fig. 1 Ring-shaped steel plate shear wall model, specimen 2-13-1 (Egorova *et al.* 2014)

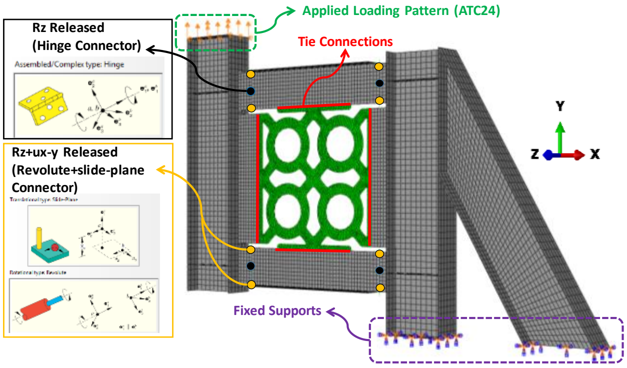

Fig. 2 Finite element modeling, definitions and boundary conditions

Roodsarabi *et al.* 2016, Khatibinia *et al.* 2018), TO of structures considering the nonlinear behavior of material (Yuge and Kikuchi 1995, Maute *et al.* 1998) and geometry (Buhl *et al.* 2000, Jung and Gea 2004, Huang and Xie 2010), implementation of TO for various elements (Tenek and Hagiwara 1994, Ansola *et al.* 2002, Long *et al.* 2009), considering multiple load cases in TO (Yi *et al.* 2013), TO of structures with regard to buckling phenomenon (Ye *et al.* 2016), and the effects of dynamic loads in TO (Liu *et al.* 2017) are some of the improvements that have led to applying TO in the complex problems and a variety of structures (Lee and Park 2001, Seyedpoor and Gholizadeh 2008, Kutyłowski and Rasiak 2014, Dehghani *et al.* 2016, Mashayekhi *et al.* 2016, Zhou 2016, Dang *et al.* 2017). Todays, professional software such as TOSCA, Genesis, Altair Hypermesh, BESO and ParamMatters are also designed for TO, and are regularly updated on the basis of the latest achievements. Also, a number of papers were presented that utilized the professional programs such as BESO (Tang *et al.* 2014), Altair Hypermesh (Tsavdaridis *et al.* 2015, Zhao *et al.* 2016, Lu *et al.* 2017) and TOSCA (Kabus and Pedersen 2012, Søndergaard and Pedersen 2014, Jansseune and Corte 2017, Bagherinejad and Haghollahi 2018) to conduct TO in the practical problems.

This study focuses on the investigation of thick PSPSWs in simple frames from two points of view. The first view is the practical application of TO in an experimental model to seek the optimal form of thick PSPSWs using TOSCA and ABAQUS. The second is a comprehensive view of the nonlinear behavior of optimized PSPSW, RS-SPSW and traditional forms of SPSWs (including infill plate, a plate with a central circular hole and plate with multi-circular holes), while the material volume of plate in all the models is constant. For this purpose, in the second section, a finite element model is presented based on the RS-SPSW experimental model. It is used as the basic numerical model for the TO and nonlinear analysis. In the third section, the TO definitions, procedure and results are presented. In the fourth section, the results of the nonlinear analysis about the optimized model and the other models are discussed.

Table 1 Material properties definition

Material	Elasticity modules (MPa)	Poisson's ratio	Yield stress (MPa)	Ultimate stress (MPa)	Ultimate strain
Shear plate	2e5	0.3	248	400	0.2
Surrounding frame	2e5	0.3	340	450	0.2

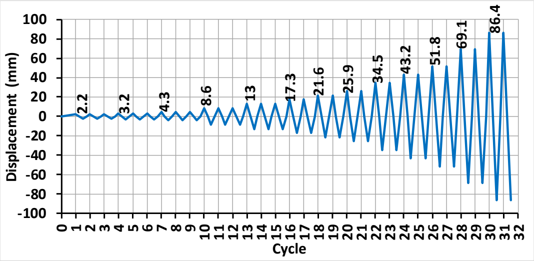

Fig. 3 ATC 24 loading pattern

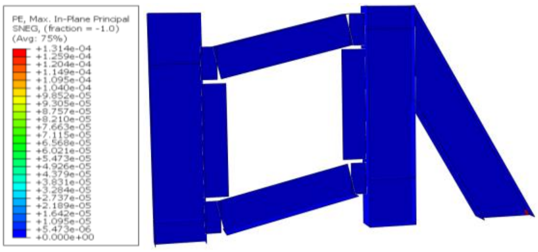

Fig. 4 Strain contour of determined pin connections

2. Numerical modeling of test specimen

In this section, a finite element (FE) method is proposed and the details are described. The FE analysis is conducted by using ABAQUS (2014). All dimensions and details are according to the experimental model that is called 2-13-1 specimen (see Fig. 1) (Egorova *et al.* 2014). The material properties of the plate and surrounding frame are assumed according to Table 1. The isotropic hardening rule is utilized for hysteresis material behavior (Maurya 2012, Maurya *et al.* 2013). It is assumed that the bolts transfer all the internal forces, so the bolts are eliminated and the elements

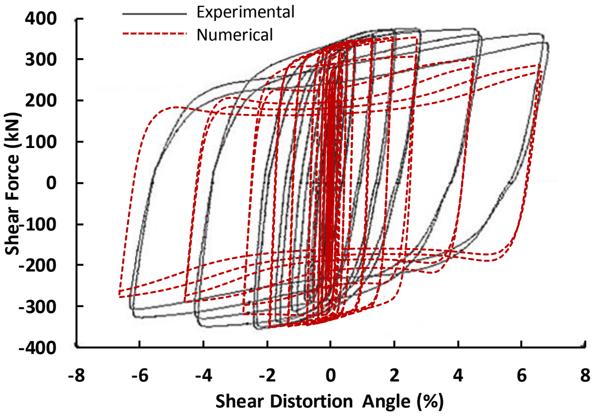

Fig. 5 Comparing load-displacement curves of numerical and experimental models

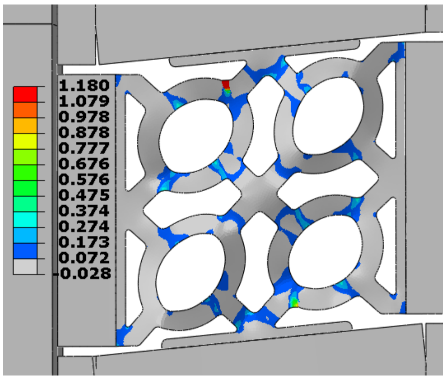

(a) Numerical model (strain contour)

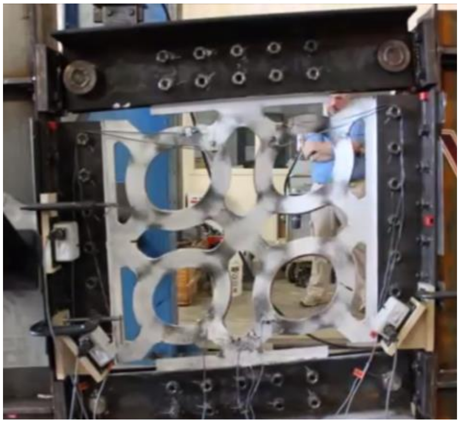

(b) Experimental model (Egorova 2013)

Fig. 6 Comparing the situation of models in the last cycle

are connected using the tie connection (see Fig. 2). All parts are meshed by the four nodes reduced integration shell (S4R) element. The dimension of elements on the plate is equal to 7mm. The dimensions of elements for angles and W12x26 are equal to 20mm and 30mm respectively.

The loading pattern is according to ATC24 (1992) protocol (see Fig. 3). The analysis is conducted in the general-static module, and the nonlinearity behavior of material and geometry are considered. The automatic stabilization is utilized to investigate the surface wrinkling, material instability and buckling using a constant damping factor. It is suitable to simulate wrinkling and buckling of steel plates (Bagherinejad and Haghollahi 2018). At each step, new values for the damping factor are calculated based on the first increment of the step and on the damping intensity (ABAQUS 2014).

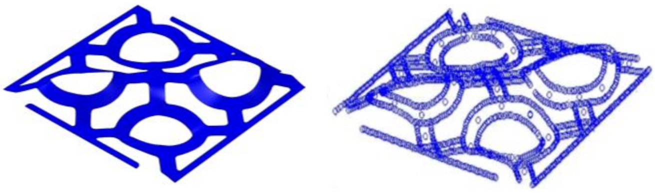

(a) Numerical model (b) Experimental model (Egorova 2013)

Fig. 7 Out-of-plane deformation in the last cycle

As seen in Fig. 1, the connection between L8×4×7/16 and W12×26 is a pin connection. For modeling a pin connection, the rotation about the z-axis (R_z) at the center should be released. In addition, the rotation about the z-axis, x-transition and y-transition ($U_{x\text{-}y}$) at the top and bottom of the web should be released. For this purpose, a hinge connector of the assembling category is used for the center of the web, and a slide-plane and revolute of the basic category are combined and applied to the top and bottom of the web (see Fig. 2). The model is analyzed without the plate to investigate the behavior of connections. As shown in Fig. 4 the results indicate that no significant stress occurs in the frame and the frame behaves the same as a simple frame.

The results of finite element model are compared with the experimental model. As shown in Fig. 5, the numerical results have suitable compliance with the experimental results reported in Ref. (Egorova 2013, Egorova *et al.* 2014). In Fig. 5, the differences between the numerical and experimental results are due to the complete condition of the finite element method, the ideal condition in the hardening model, the ideal condition of the connector in comparison with the pin connection and using the tie connection replacing the bolt connections. In Fig. 6, the strain distribution at the end of loading is compared with the experimental model. The results show that the numerical model predicts well the strains created in the experimental model. In Fig. 7, the out-of-plane deformation of the experimental and numerical models is compared. As can be seen, the obtained deformation from the finite element analysis corresponds well to the experimental model.

3. Topology optimization

TO is a mathematical method that optimizes the material configuration within a given design space, objective function, set of loads, boundary conditions and constraints. TO of solid structures involves the specification of features such as the number, location and shape of holes and connectivity (Bendsøe and Sigmund 2003). TO could be written in a general form of a problem as Eq. (1) (Hassani and Hinton 1999):

$$\begin{gathered} \textit{Optimize } \Psi(x) \\ \textit{Such that}: \begin{cases} h_j(x) = 0 & j = 1, 2, \ldots, d_h \\ g_k(x) \le 0 & k = 1, 2, \ldots, d_g \\ x_l^i \le x_i \le x_u^i & i = 1, 2, \ldots, d \end{cases} \end{gathered} \tag{1}$$

where Ψ is the objective function, h_j and g_k are the quality and inequality constraint functions, d_h, d_g and d are the number of equality constraints, inequality constraints and design variables, respectively. The values x_l^i and x_u^i are the lower and upper bounds on a typical design variable x_i (element density).

3.1 Objective function and loading pattern

Defining the objective function is the first and most important step in an optimization problem. Also, there are several factors such as optimization target, type of structure, loading pattern, solution method, etc. that are effective in determining the objective function. In this study, the main target of TO is to improve the stiffness and ductility of the PSPSW simultaneously. Stiffness and ductility are two effective parameters on the dynamical behavior of a structure. However, increasing the stiffness without considering the ductility causes the fracture tendency in a structure to increase. Therefore, the primary challenge is the selection o an objective function in such a way that the effects of both stiffness and fracture tendency are taken into account. There are several different objective functions to maximize the structural stiffness such as strain energy, eigenfrequency, reaction force and etc. Each objective function has some limitations. For example, the application of nonlinear analysis is not possible for eigenfrequency or the use of cyclic loading doesn't impact on the optimization based on the strain energy (TOSCA 2013). Herein, an objective function is required that has the minimum limitations. In this paper, the maximization of reaction forces is applied as the objective function because of the following reasons including (I) applying the nonlinear analysis (nonlinearity in material, geometry and buckling) in TO, (II) applying a cyclic loading in TO and (III) possibility of optimization based on the last cycle of loading. Considering the static equilibrium ([stiffness]×[displacement]=[force]) and given that the load will be imposed to the structure as a displacement, the reaction forces should be maximized to increase the stiffness according to Eq. (2).

$$\max : \Psi = \sum K_q U, \quad U = K^{-1} F, \; where \; K = \sum x_e^p k_e \tag{2}$$

where q is the node or nodes that constrained by the fixed support (the nodes in the fixed support zone). K_j corresponds to a row of the global stiffness matrix (K) that belongs to the node q considering to the loading direction, U is the global displacements vector, F is the global external forces vector, k_e is the element stiffness and p is the penalization power.

It is proved that in the moment frames, the optimized plate is obtained by a loading displacement equal to 10% drift. In the moment frame, the effects of strength degradation due to pinching behavior are compensated by the moment connections. So, there is no significant strength degradation in the pinching and tension zones in each cycle of loading (Bagherinejad and Haghollahi 2018). As shown in Fig. 5, the strength is degraded in each cycle of loading because of buckling in the plate. So, two loading patterns are proposed for the TO process. The first pattern is a simple monotonic loading displacement equal to 10% drift (86.4mm). The second pattern is a cyclic loading in order to consider the fracture tendency and strength degradation in the TO (see Fig. 8). As shown in Fig. 8, TO is conducted based on the last step of loading. In fact, in each iteration of TO, the cyclic loading is imposed on the structure and TO is done based on the maximization of the sum of reaction forces in the last cycle of loading when the buckling and plastic strain are completely occurred in the plate. It will cause the buckling effects, pinching behavior and nonlinear behavior of the structure to be accounted with more intense when the reaction forces are maximized. In both loading patterns, the buckling and nonlinearity effects of material and geometry are considered during TO.

3.2 Constraints and conditions

Since the optimization results should be compared with the RS-SPSW, the area of the optimized plate is a constraint that should be equal to or less than the area of RS-SPSW (314423.23mm^2). Therefore, the volume fraction (f) in each iteration of TO is equal to 0.54 times of the original volume (V_0) as follows:

$$Constranits: \begin{cases} \dfrac{V(x)}{V_0} \le f \\ 0 \le x_{\min} \le x_e \le 1 \end{cases} \tag{3}$$

where $V(x)$ is the design domain volume and $x_{\min}$ is the lower bound of element density. In order to avoid a singularity in the global stiffness and re-meshing, a lower $x_{\min}$ bound should be set for the element density (x_e). Obviously, the upper bound is equal to 1. The lower bound is determined equal to 0.001. The total number of iterations is equal to 100 and at least 4 iterations should be done to terminate the TO. In addition, two stop criterions (the rate of change in the objective function ($l_1 \le 0.001$) and rate of change in the volume ($l_2 \le 0.003$)) are defined in order to prevent doing of extra iterations according to Eq. (4).

$$Stop\ Conditions: \begin{cases} n > 100 \\ l_1 = \dfrac{|\Psi_{n+1} - \Psi_n|}{|\Psi_{n+1}|} \le 0.001 \\ l_2 = \dfrac{|x_{n+1} - x_n|}{N} \le 0.003 \end{cases} \tag{4}$$

where n and N are the number of iterations and total number of elements, respectively. Due to the cyclical nature of seismic loads, a planar symmetry about the X and Y axis at the center of the plate is considered in TO.

3.3 Algorithm and solution method

TO has three main steps. In the first step, the effective elements are recognized using sensitivity analysis ($\partial\Psi/\partial x_i$). In the second step, the stiffness and density of effective elements are increased and the density and stiffness of ineffective elements are decreased. It should be noted that no element is eliminated. The element elimination led to re-meshing the structure in each iteration of TO and it is very

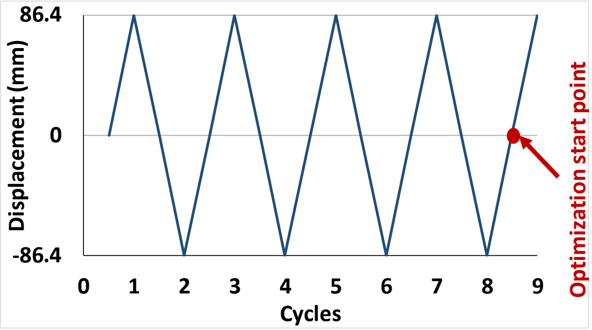

Fig. 8 Determined cyclic loading for optimization

time-consuming. So, an element is graphically deleted when the element density is less than $x_{\min}$ (Bendsøe and Sigmund 2003, TOSCA 2013). This interpolation between the density and stiffness is conducted by SIMP (Simple Isotropic Material with Penalization) method based on the density x^m and stiffness E^m in iteration m respect to the original density x^0 and stiffness E^0 in iteration 0 as written in Eq. (5) (Bendsøe 1989). In the third step, the objective function is updated using the method of moving asymptotes (MMA) according to Eq. (6) in iteration m (Svanberg 1987).

$$E^m = E^0 \left(\frac{x^m}{x^0} \right)^p \tag{5}$$

$$MAX : \Psi = \Psi(x^m) - \sum_{e=1}^{N} \left(\frac{\left(x_e^m - L_e \right)^2}{x_e - L_e} \times \frac{\partial \Psi}{\partial x_e} \left(x^m \right) \right) \tag{6}$$

where p is the penalization power, according to the SIMP method and L_e is the lower of vertical asymptotes for the approximations of Ψ. The numerical results of previous studies indicate p=3 is a suitable value (Bendsøe and Sigmund 2003). A flowchart is presented in Fig. 9 to indicate the TO process.

3.4 Topology optimization results

For TO a numerical model according to the experimental model is prepared with an infill plate (see Fig. 10). The finite element modeling is based on the proposed model in the second section. As shown in Fig. 10, the size of a rectangle (131mm×25.5mm) is removed from the corners of the infill plate because the frame should behave as a simple frame with the hinge connections. The TO is conducted for 12.7mm and 6.4mm plate thicknesses and under the monotonic and cyclic loadings. The defined thicknesses are based on the experimental model (Egorova *et al.* 2014). The summary of TO definitions and results is presented in Table 2.

Fig. 10 indicates the density ratio of all elements is equal to 0.54 (based on the prescribed volume fraction) of the original density of elements in the first iteration of TO. In the next iterations, by using MMA and SIMP method the density of the elements is modified and updated based on the values of the objective function. The results of the objective function and volume fraction during TO iterations for the models are presented in Fig. 11. The total number of iterations for OPT6M, OPT12M, OPT6C and OPT12C reached to 31, 28, 42 and 64 respectively. It indicates TO is stopped without reaching the iteration 100 because the stop criterions are satisfied.

Table 2 Optimization definitions and results

Model name	Loading Patter	Plate Thickness (mm)	Initial volume fraction	Final volume fraction	objective function	objective function	Number of iteration
OPT6M	Mono	6.4	0.54	0.539	164	537	31
OPT12M	Mono	12.7	0.54	0.539	272	889	28
OPT6C	Cyclic	6.4	0.54	0.539	167	295	42
OPT12C	Cyclic	12.4	0.54	0.539	279	608	62

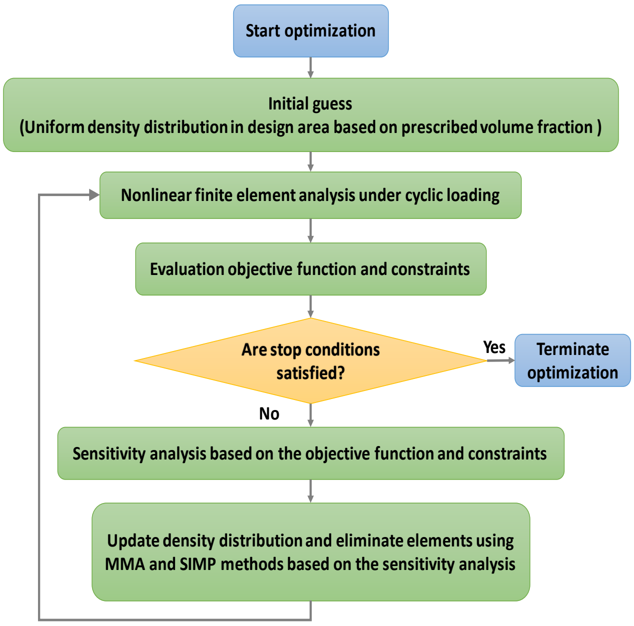

Fig. 9 Topology optimization procedure flowchart

The changes of configuration during TO iterations are shown in Fig. 12 and Fig. 13 for monotonic and cyclic loading, respectively. It can be seen from Fig. 12 and Fig. 13 that the plate thickness has a tiny effect on the TO results. As expected, the results of TO under the monotonic loading are different from the TO under the cyclic loading. The concept of optimized form under monotonic loading is similar to the plate with a circular hole. It indicates that the plate with a central hole could be an optimized form. So in the next section, the plate with a circular hole replaces the optimized form under the monotonic loading. By comparing and matching the optimized plates under cyclic loading (OPT6C and OPT12C), an optimal form for both thicknesses is proposed using AUTOCAD (see Fig. 14). Given the similarity of the proposed shape to the sun, the optimal shape is called solar-shaped steel plate shear wall (SS-SPSW). It should be mentioned that the area of the plate in the SS-SPSW is equal to the RS-SPSW. The results show the obtained forms at the end of TO are clear and the density of most elements is reached to x_e=1. It proves the

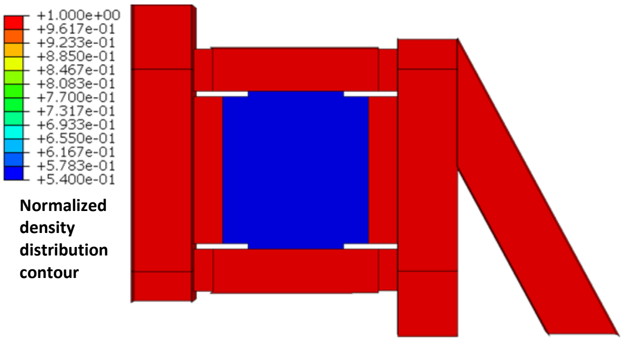

Fig. 10 Density distribution in the first iteration

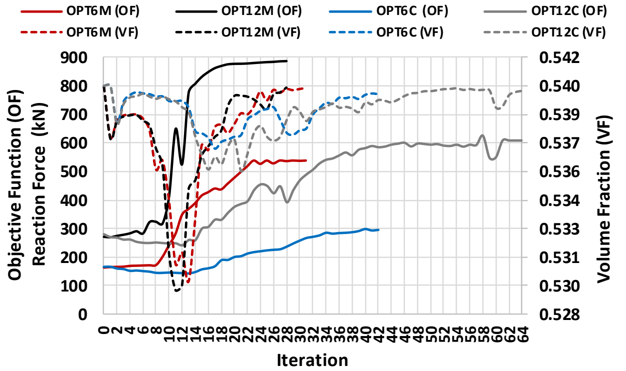

Fig. 11 Objective function and volume fraction during TO iterations

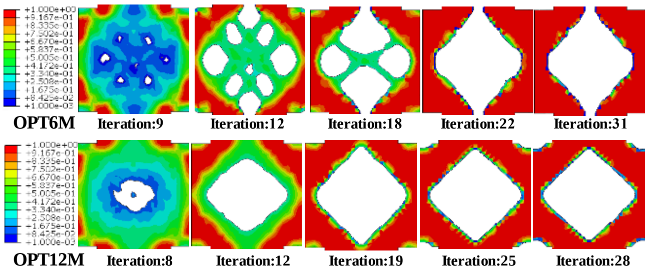

Fig. 12 Configuration changes of plate during TO iterations under monotonic loading

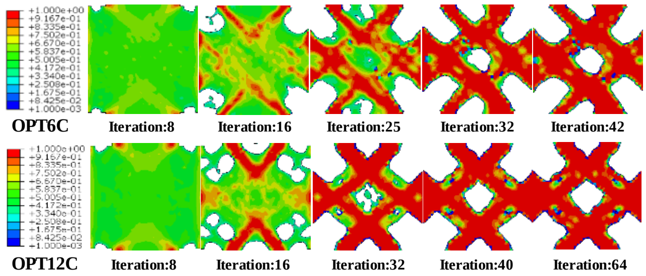

Fig. 13 Configuration changes of plate during TO iterations under cyclic loading

defined values for stop conditions are suitable. Also, the results illustrate well the use of nonlinear analysis in TO prevents from creating slim parts in the configuration.

4. Nonlinear behavior of SS-SPSW

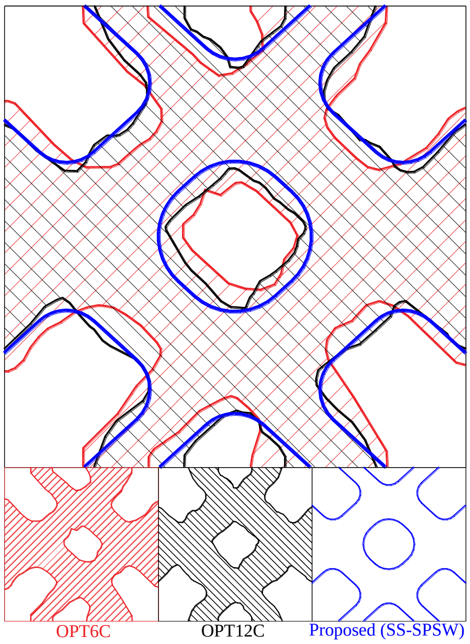

Fig. 14 Proposed optimal form of perforated plate

In this section, for a comprehensive comparison, the nonlinear behavior of the SS-SPSW model under cyclic and monotonic loadings is studied and compared with the RS-SPSW and four usual form of SPSWs for both 6.4mm and 12.7mm thicknesses (see Fig. 15 and Table 3). As seen in Fig. 15, a plate with one central circular hole (CP model), aplate with four circular holes (2CP model) and a plate with nine circular holes (3CP model) are proposed. Also, an infill plate with less thickness, but a similar volume is presented (FP model). The volume of the plate in all the models is approximately equal (see Table 3). The cyclic loading is imposed according to ATC24 that was presented in the second section. The monotonic loading is applied to the structures as a displacement in the up direction. The amount of imposed displacement in the monotonic loading is equal to 86.4mm (10% drift).

4.1 Cyclic and monotonic behavior

The curves of load-displacement of all the models for both thicknesses are presented in Fig. 16. The cyclic hardening behavior of the material causes the monotonic curves to appear below the cyclic curves in the initial cycles (Wang *et al.* 2015). By increasing the number of cycles and consequently the increase of out-of-plane deformation, buckling and plastic deformations, the monotonic curves appear at the top of the cyclic loading. As seen in Fig. 16, for SS12, RS12, 2CP12 and 3CP12 the monotonic curves are below the cyclic curves in the initial cycles and gradually move to the top of the cyclic curves. With decreasing thickness of the plate, the effects of material hardening in the cyclic loading are reduced and the monotonic curves are approximately located above the cyclic curves (see models SS6, RS6, FP3, CP6, 2CP6 and 3CP6 in Fig. 16). The pinching behavior of the SS12 model is similar to the 2CP12 model. There is also a similarity between the pinching behavior of RS12 and 3CP12. In CP12, a reduction in resistance is observed in the initial cycles. Despite the increase of resistance in the FP6 model,

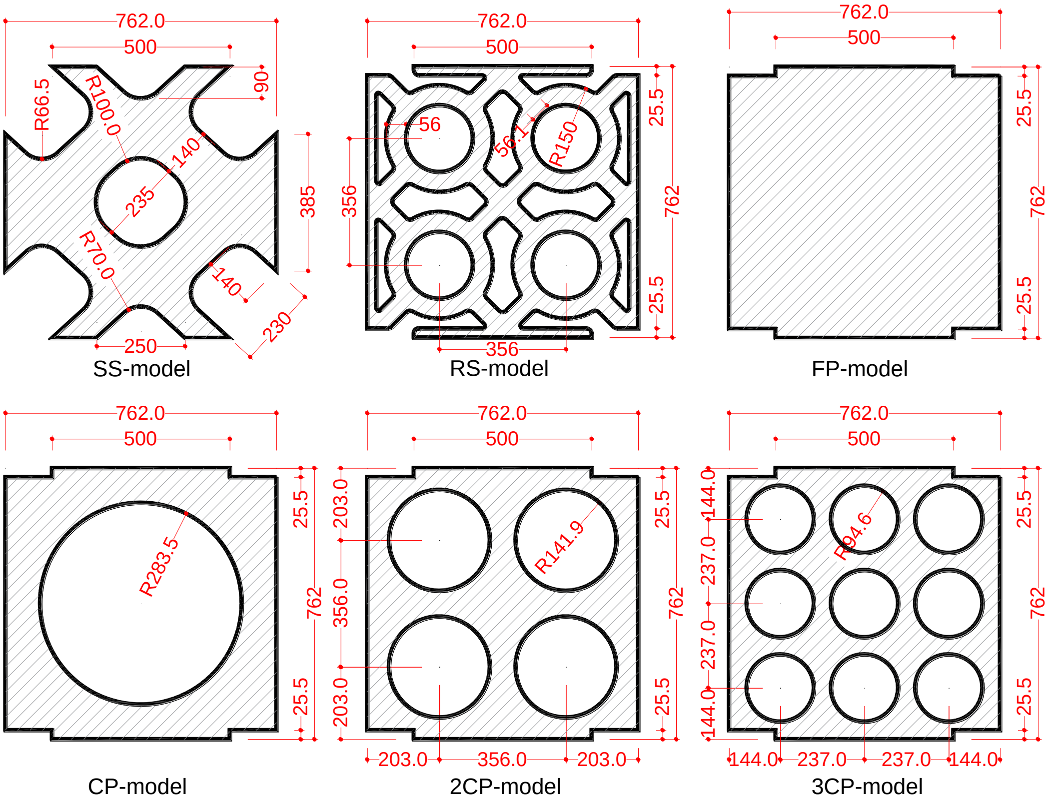

SS-model RS-model FP-model

CP-model 2CP-model 3CP-model

Fig. 15 Dimensions of plates (all dimensions are in mm)

Table 3 Name and properties of plates

Basic model	Area (mm^2)	Model name	Thickness (mm)	Volume (mm^3)
SS model	314493	SS12	12.7 (Thicket plate)	3994061
		SS6	6.4 (Thinner plate)	2012755
RS model	314423	RS12	12.7 (Thicket plate)	3993172
		RS6	6.4 (Thinner plate)	2012307
FP model	567282	FP6	6.4 (Thicket plate)	3630605
		FP3	3.2 (Thinner plate)	1815302
CP model	314785	CP12	12.7 (Thicket plate)	3997770
		CP6	6.4 (Thinner plate)	2014624
2CP model	314286	2CP12	12.7 (Thicket plate)	3991432
		2CP6	6.4 (Thinner plate)	2011430
3CP model	314303	3CP12	12.7 (Thicket plate)	3991648
		3CP6	6.4 (Thinner plate)	2011539

the curve is not smooth and in fact, an instability in stiffness and strength is repeatedly observed due to wrinkling and buckling in the plate. This is also observed in the FP3 model with more intensity (see Fig.18). Therefore, it can be said that in the PSPSWs, the plastic deformation occurs in a specific and regular patch and the reduction rate of strength and stiffness in each loop is regular and soft in comparison to the infill model. Note that the instability in stiffness of the shear plate is compensated in a frame by the moment connections and the stiffness of connections causes this instability isn't observed, but it is clearly observable in a frame with simple connections. By reducing the thickness of the plate, it is obvious that the pinching behavior becomes weaker.

The push of cyclic curves is presented in Fig. 17 that indicates the envelope of tension field action of the models. The push of the cyclic curve for the SS model (for both thicknesses) has the highest value after the FP model. In all the perforated models with the thicker plate (SS12, RS12, CP12, 2CP12, 3CP12) a decrease in the strength is observed in the initial cycles. In RS12 and RS6 this reduction is minimum. The strength reduction in the initial cycles of models with the thinner plate (SS6, RS6, FP3, CP6, 2CP6, 3CP6) is considerably decreased. In the models with the thicker plate, the difference of strength before and after buckling is more than the models with the thinner plate. Therefore, the strength reduction in the initial cycles of models with the thicker plate is more than the thinner plate.

For investigating the pinching behavior of models, the load-displacement curve of the models in the last loop is shown in Fig. 18. The results illustrate that the perforated models approximately have similar strength in the pinching zone. In the tension field action zone, the SS model has higher strength than the other perforated plate for both thicknesses. As mention prior, the load-displacement curve

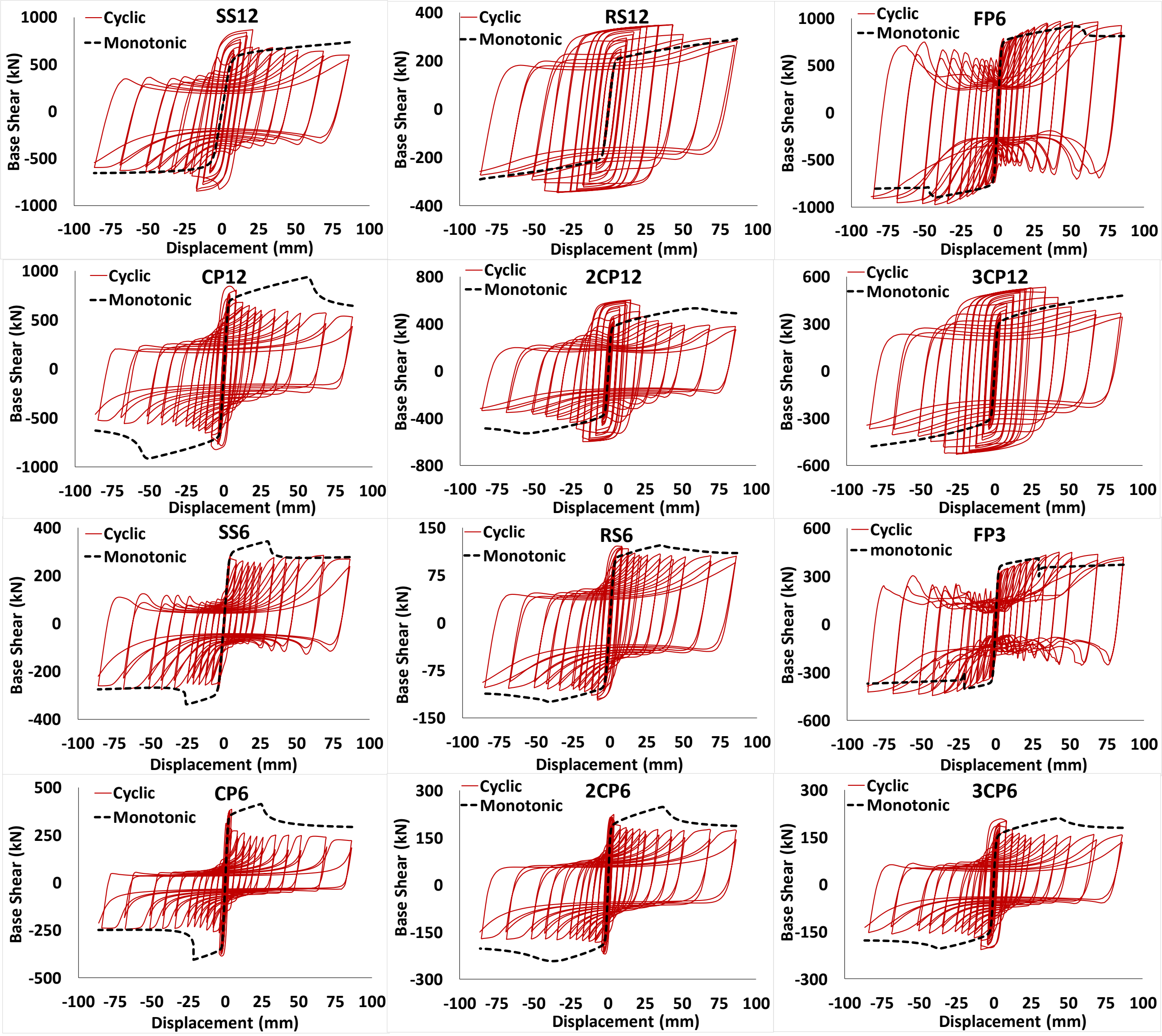

Fig. 16 Load-displacement curve for cyclic and monotonic loadings

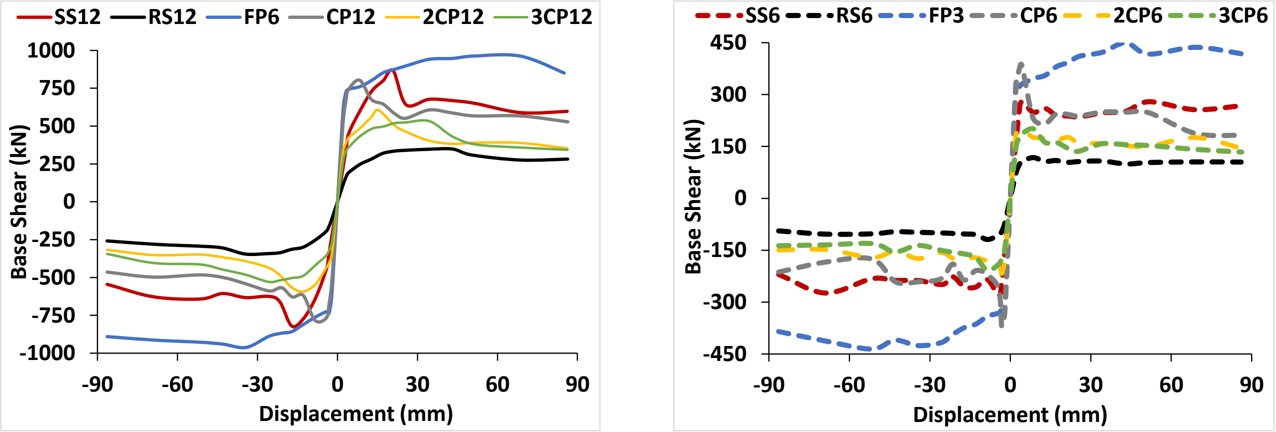

(a) Models with thicker plate

(b) Models with thinner plate

Fig. 17 Push of load-displacement curve in cyclic loading

for the FP models has an instability in stiffness because of wrinkling and buckling in the plate that occur repeatedly. As shown in Fig. 18, the minimum strength of FP6 in the pinching zone is less than SS12.

A comparison of the monotonic curve of the models is presented in Fig. 19. In FP6, CP12, and 2CP12 a strength reduction occurs due to buckling of the plate. In SS12,

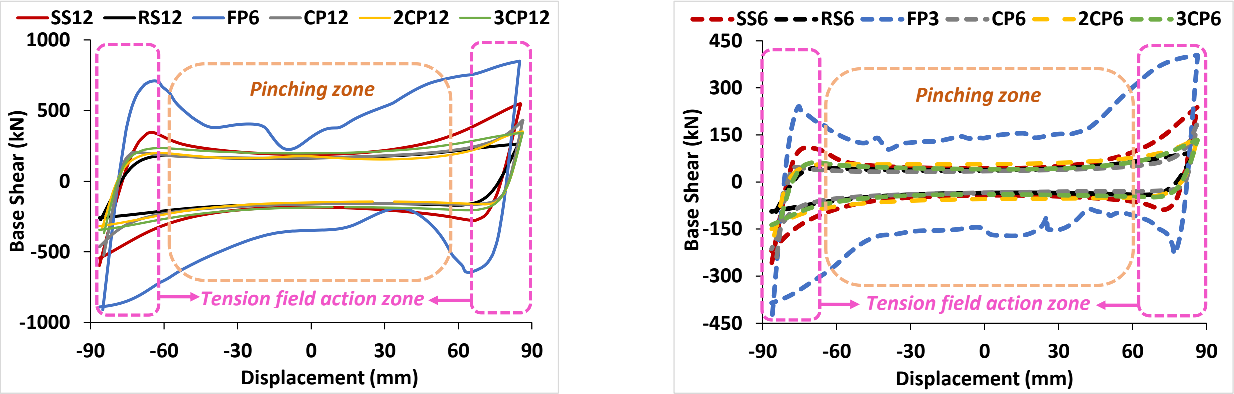

(a) Models with thicker plate (b) Models with thinner plate

Fig. 18 Load-displacement curve in the last loop

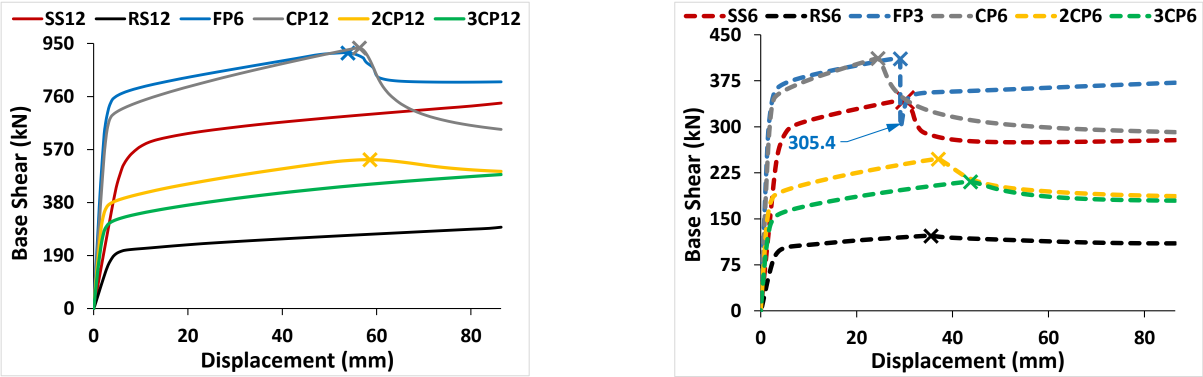

(a) Models with thicker plate (b) Models with thinner plate

Fig. 19 Load-displacement curve for monotonic loading

RS12 and 3CP12 no strength reduction occurs during loading. The starting point of strength reduction is marked with a symbol (×). The strength of CP12 after 67mm displacement is less than SS12. In 2CP12, buckling occurs at 58mm displacement and the strength reduces. The buckling and consequently the strength reduction are observed in all the models with the thinner plate. The strength of FP3 at 29mm displacement considerably reduces to 305.4kN and the curve is located below SS6 at this point. The strength reduction in CP6 is considerable and the curve of CP6 approximately reaches to the SS6 at the end of loading.

4.2 Load-carrying capacity

Given the presented cyclic and monotonic curves in Fig. 16, it can be seen that the load-carrying of the SS model is significantly increased in comparison with the other perforated plates. Based on the monotonic curves, the amounts of reaction force of yield point (P_y), maximum reaction force (P_{max}) and the ultimate reaction force according to the maximum deformation (P_u) are calculated (see Fig. 20). According to the cyclic loading, the maximum reaction force (P_n) is determined. Based on the load-displacement curve in the last loop (see Fig. 18), the maximum strength in tension field action zone (P_1) and minimum strength in the pinching zone (P_2) are calculated.

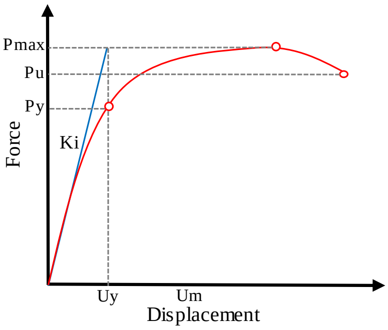

Fig. 20 Defined method for strength capacity in monotonic loading

The amounts of strength and load-carrying are presented in Table 4. Also, the ratios of these parameters with respect to the SS model are calculated and presented in Fig. 21. It can be seen from Table 4 and Fig. 21 that the FP model has the highest amount in the strength, but the behavior of this model is accompanied by an instability in stiffness and severe drop in strength as mentioned previously. Therefore, in the following the discussion is presented about the perforated plates. In the perforated plates, SS12 and SS6 have the highest strength in the tension action zone (P_1). The values of P_2 for the models with the thicker plate are near to each other. The value of P_2 for 3CP12 is 1.0015 times that of SS12. In the models with the thinner plate, P_2 for 2CP6 is 1.25 times that of SS6. In the maximum

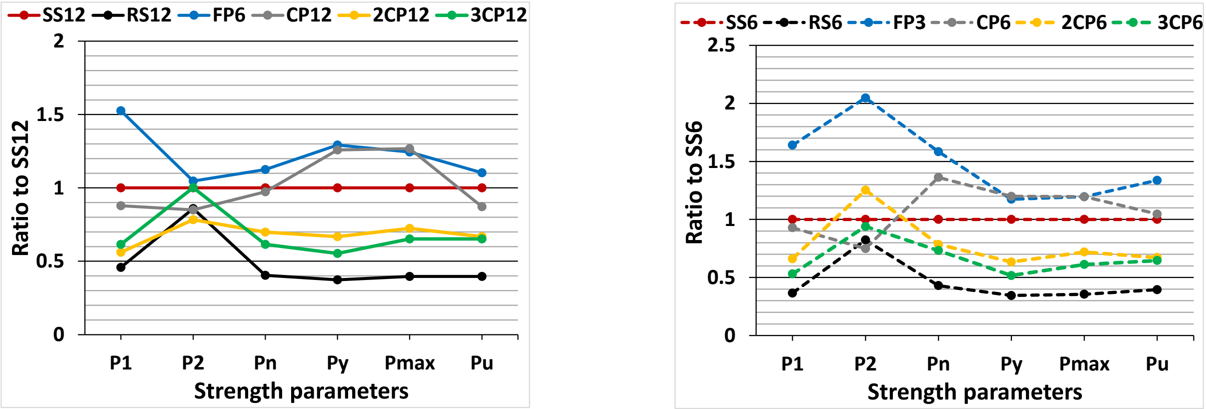

(a) Models with thicker plate (b) Models with thinner plate

Fig. 21 Ratios of load-carrying parameters with respect to SS models

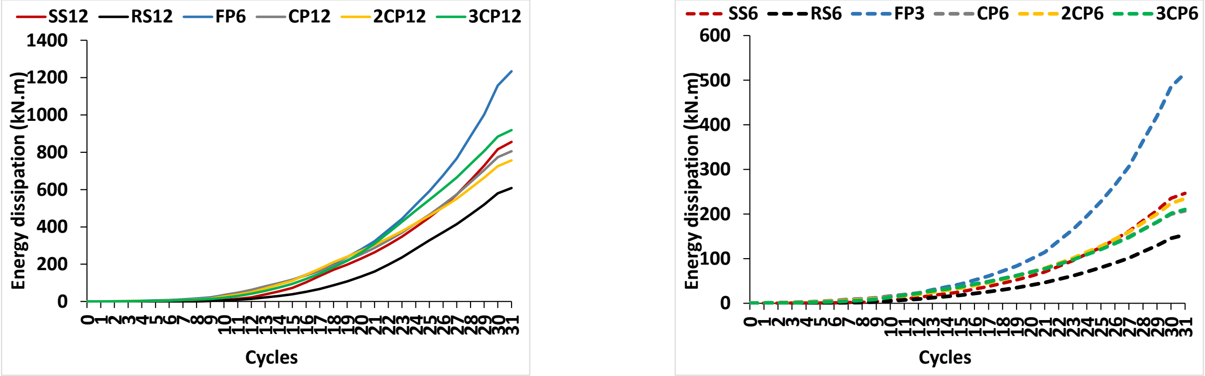

(a) Models with thicker plate (b) Models with thinner plate

Fig. 22 Energy dissipation curves

Table 4 Values of load-carrying capacity (kN)

Models	P1	P2	Pn	Py	Pmax	Pu
SS12	596.53	183.59	865.66	546.31	736.67	736.67
RS12	273.09	157.82	350.02	203.69	291.73	291.73
FP6	910.53	192.23	974.50	706.29	917.47	812.66
CP12	523.90	155.99	843.04	687.62	934.07	642.25
2CP12	334.71	143.87	605.13	364.70	533.69	491.66
3CP12	367.08	183.87	532.67	302.36	480.47	480.47
SS6	257.63	42.37	284.05	279.16	343.93	278.11
RS6	94.31	34.87	122.17	96.40	122.28	109.97
FP3	422.64	86.72	449.98	327.78	411.25	371.86
CP6	239.37	31.77	386.95	334.81	411.46	291.16
2CP6	170.55	53.07	223.13	177.03	247.31	186.92
3CP6	136.85	39.82	207.91	144.44	210.44	179.76

strength of the cyclic loading field (P_n), SS12 has the highest value of P_n. The value of P_n for CP6 is 1.36 times that of SS6. The values of P_y for CP12 and CP6 are 1.26 and 1.17 times that of SS12 and SS6 respectively. In the maximum reaction force field (P_{max}), SS12 and SS6 have the highest value after CP model. The values of P_{max} for CP12 and CP6 are respectively 1.24 and 1.19 times that of SS12 and SS6. In the ultimate reaction force field (P_u), SS12 has the highest value. The amount of P_u for CP6 is 1.05 times that of SS6.

4.3 Energy dissipation

The area under a load-displacement curve is equal to the energy dissipation (ED). So, the dissipated energy of a structure is a composite index of stiffness and ductility. The ED of all the models is presented in Fig. 22. The values of ED and differences between ED curves of the models are ignorable up to the 9th cycle for both thicknesses. The ED of the FP model is considerably more than the other models. Also, the ED curves of the RS model are located in the lowest position. The ED curve of SS, CP, 2CP and 3CP are in a limited bound. For models with thicker plate, after the FP6 model, 3CP12 has the highest ED capacity. After the 26th cycle, the energy dissipated by SS12 is higher than the CP12 and 2CP12 models. After the 24th in the models with the thinner plate, the energy dissipated by SS6 is higher than the CP6, 2CP6 and 3CP6 models. The values of ED at the end of cyclic loading are presented in Table 5. The values of ED at the end of cyclic loading for FP6 and 3CP12 are respectively 1.44 and 1.073 times that of SS12 and for FP3 is 1.6 times that of SS6.

4.4 Fracture tendency

Increasing the stiffness and strength capacity would be useful if it didn't cause the fracture tendency to increase and the ductility to reduce. The fracture tendency can be predicted by equivalent plastic strain (PEEQ). PEEQ is

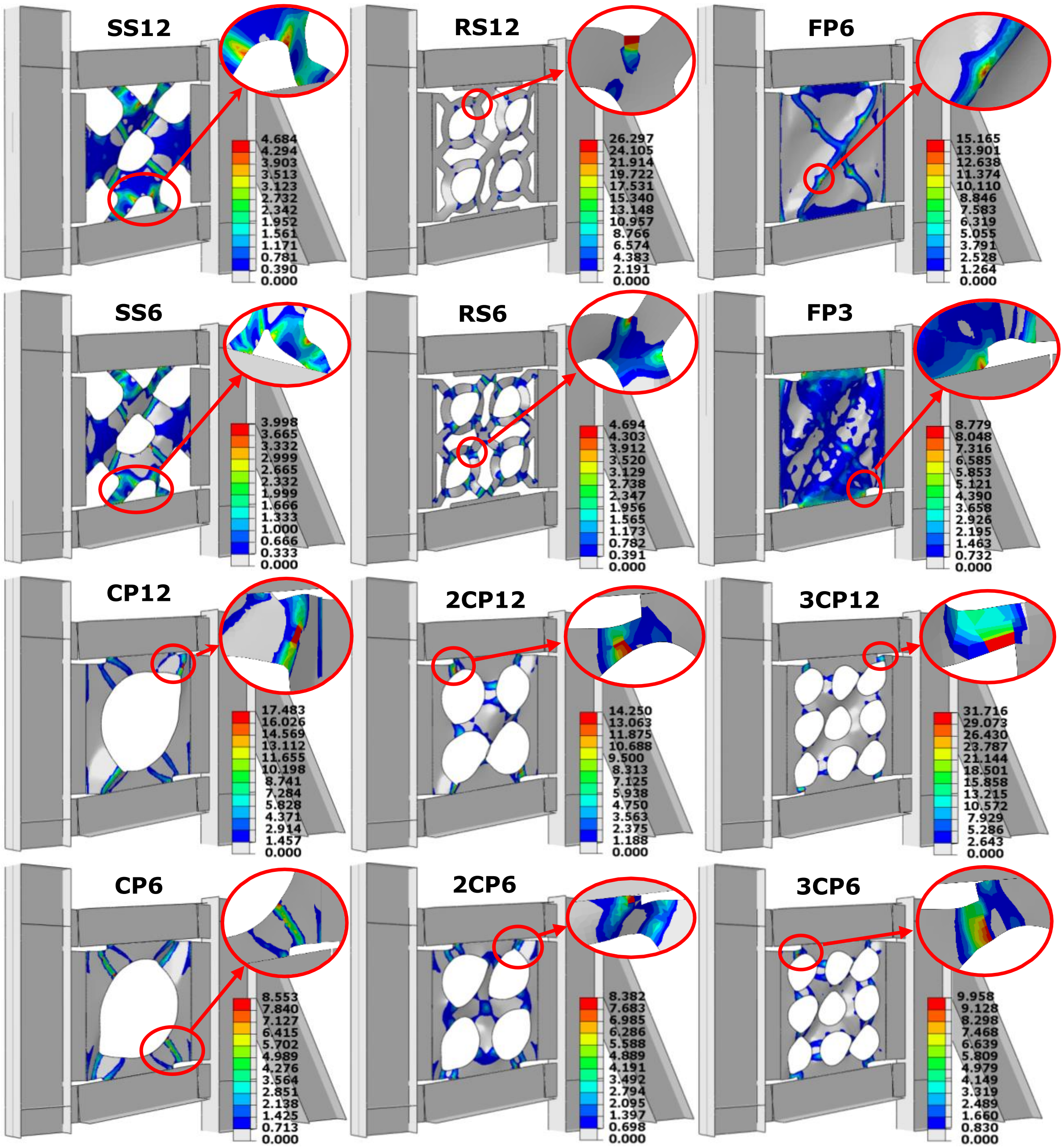

Fig. 23 Equivalent plastic strain distributions, contours and failure modes at the end of cyclic loading

described as a cumulative variable and a monotonically incremental function. This index represents the local damage and fracture tendency of steel (ABAQUS 2014, Wang *et al.* 2015, Bagherinejad and Haghollahi 2018).

Fig. 23 shows the locations of PEEQ and failure modes. It can be seen from Fig. 23 that for FP3, CP12&6, 2CP12&6 and 3CP12&6 models, maximum PEEQ is located in the corner of the plate where the plate is connected to the frame. Also, for the RS models, the plastic strain appears in the corner of the ring. The values of PEEQ for all the models are presented in Table 5. The numerical results show that in the SS12 and SS6 models, PEEQ is significantly reduced in comparison to the other models. In the models with the thicker plate, maximum and minimum of PEEQ belong to 3CP12 (31.716) and SS12 (4.684) respectively. After the SS12 model, 2CP12 has the lowest value of PEEQ (14.25). Therefore, in comparison to the other models, in SS12 the PEEQ is reduced nearly 67% to 85%. The SS6 (3.998) and 3CP6 (9.958) have the minimum and maximum PEEQ in the models with the thinner plate.

The PEEQ reduction of SS6 in comparison to RS6 and 3CP6 is nearly 15% and 60% respectively. As expected, the amounts of PEEQ with decreasing thickness of the plate is reduced for all the models. It can be seen from Fig. 23 that the stresses and consequently the equivalent plastic strains have appropriate distribution in the plate of SS model. It

Table 5 Energy dissipation and equivalent plastic strain (PEEQ) at the end of cyclic loading

Models	Energy dissipation (kN.m)	PEEQ	ED/PEEQ
SS12	855.86	4.684	182.72
RS12	607.77	26.297	23.11
FP6	1233.85	15.156	81.41
CP12	805.21	17.480	46.06
2CP12	755.93	14.250	53.05
3CP12	918.71	31.716	28.97
SS6	246.39	3.998	61.63
RS6	153.35	4.694	32.67
FP3	515.64	8.779	58.74
CP6	207.12	8.553	24.22
2CP6	234.49	8.382	27.98
3CP6	210.16	9.958	21.10

causes a reduction in PEEQ in comparison to the other models.

The ratio of energy dissipation to PEEQ (ED/PEEQ) represents the capability of the models against the seismic and wind loads (see Table 5). The results indicate the capability of SS models is impressively increased in comparison to the other models. As shown, this enhancement on average is equal to 377% for 12.6mm thickness and 112% for 6.3mm thickness.

4.5 Summary of SS-SPSW nonlinear behavior

The results show that buckling and wrinkling of the plate in the SPSW with an infill plate (FP model) creates an instability in stiffness and strength under the cyclic loading. Also, in the monotonic loading, a considerable strength reduction is observed for both thicknesses. Therefore, the FP model is not suitable for the frames with the simple connection. In comparing with the perforated models (RS, CP, 2CP and 3CP) the following results are observed about the SS model. The SS model has the best behavior in the push of cyclic loading and tension field action. Also in the pinching zone, it has an appropriate performance. In the monotonic loading with the thicker plate the SS model has the highest strength capacity with no strength reduction; and with the thinner plate, it has a higher strength capacity than the 2CP, 3CP and RS models. In the energy dissipation field, it has an appropriate behavior. In the models with the thicker plate at the end of loading, the energy dissipated by 3CP12 is 1.073 times of SS12; On the other hand, the fracture tendency of 3CP12 is 6.77 times of SS12. SS6 has the highest value of energy dissipation at the end of loading in the models with the thinner plate. In the fracture tendency field, it is shown that the amount of equivalent plastic strain (PEEQ) is significantly decreased in the SS model. Therefore, the results prove that the SS model has a suitable capacity in load-carrying, energy dissipation and fracture tendency.

Table 6 Statistics of conducted exams

Plate thickness (mm)	Item	Number of total exams	Number of successful exams	Average of improvements (%)	Number of failed exams	Average of deterioration (%)
12.6	SC	12	12	49.2	0	-
	SM	12	10	81.3	2	-20.8
	ED	4	3	20.1	1	-6.8
	FT	4	4	-76.9	0	-
6.3	SC	12	10	57.8	2	-23.4
	SM	12	9	97.9	3	-12.5
	ED	4	4	25.5	0	-
	FT	4	4	-45.1	0	-

SC: Strength under Cyclic loading (P1, P2, Pn)
SM: Strength under Monotonic loading (Py, Pmax, Pu)
ED: Energy Dissipation
FT: Fracture Tendency (PEEQ)

For a better comparison, the results of the analysis are presented statistically (see Table 6). There are eight items were considered to evaluate the performance of optimized plate including structural resistance (6 items: P1, P2, Pn, Py, Pmax, Pu), energy dissipation (ED) and fracture tendency (PEEQ). Also, these items were evaluated for three traditional forms of PSPSWs and the ring-shaped model. So, there are 32 exams that were conducted for the optimized model for each thickness (12.6mm and 6.3mm). For example, as shown in Table 6, the energy dissipation of SS12 is compared with the other perforated models. So, there are 4 exams in total for the optimized model. In 3 exams, the energy dissipation of the SS12 model is higher than the perforated models. This increase is on average 20.1%. But, in an exam, the SS12 model doesn't increase the energy dissipation. There is a decrease in average -6.8% in comparison to the 3CP12 model. Note that the negative and positive signs indicate the decrease and increase of values, respectively. The results of Table 6 illustrate that the optimized model has 56 successful results from 64 conducted exams.

5. Conclusion

This paper indicated the ability of topology optimization to present the new form of perforated plates in frames with simple connections based on the maximization of the reaction forces as the objective function. The use of nonlinear analysis and cyclic loading in the optimization led to creating a special form of the perforated plate that called solar-shaped steel plate shear wall (SS-SPSW). Investigating the nonlinear analysis of SS-SPSW with the other form of SPSWs proved the appropriate behavior of SS-SPSW in strength and ductility. The following topics present the main results of TO and comprehensive review in the conducted nonlinear analysis.

- The results of optimization illustrated the change in the plate thickness has an ignorable effect on the TO results.

- The nonlinear analysis (buckling and nonlinearity in material and geometry) in the TO prevented from creating slim parts in the optimized plates.
- The results of TO under monotonic loading were completely different from the TO under cyclic loading. The overall form of optimized plate under monotonic loading (OPT6M and OPT12M) was similar to the plates with a central circular hole.
- The TO process under cyclic loading and optimization based on the last cycle (considering the nonlinear behavior and buckling) led to creating a special form of PSPSW. The results showed that in the optimized model, the structural resistance and energy dissipation were improved while the fracture tendency was significantly decreased, in comparison to the other perforated and ring-shaped models. The results proved that the proposed TO process was successful in the improvement of stiffness and ductility.
- The statistics results illustrated that the optimized model had 56 successful results from 64 conducted exams. The average improvements in the strength under cyclic loading, strength under monotonic loading and energy dissipation were equal to 53.5%, 89.6% and 22.8% respectively (for both thicknesses 12.6mm and 6.3mm). On the other hand, the average reduction of fracture tendency was equal to 61%.
- The wrinkling and buckling in the infill plate caused an instability in the stiffness and strength occurred in the pinching zone. Also, the infill plate had a significant reduction (under the monotonic loading) in the strength near to 13% (for 12.6mm) and 34% (for 6.3mm) while the strength reduction for the optimized plate was near to 0% (for 12.6mm) and 23% (for 6.3mm). In addition, the values of fracture tendency (PEEQ) of FP6 and FP3 were equal to 15.165 and 8.779 while these values for SS12 and SS6 are equal to 4.6 and 3.998. So, the use of infill plates in the frame with simple connections isn't recommended.
- The pinching behavior of the 3CP12 model was desirable and very close to the ring-shaped model. The strength under cyclic loading and monotonic loading were enhanced on average near to 35% and 59% in comparison to the ring-shaped model (RS12). The energy dissipation of 3CP12 was increased by 51% respect to the RS12 model. So, the use of 3CP12 replacing the ring-shaped model is reasonable considering the difficulties and costs in the fabrication of the ring-shaped plate.
- With the decrease of plate thickness, the strength reduction and pinching behavior were increased. So, the use of perforated plate with a high thickness in the simple frame is more desirable.

References

ABAQUS (2014), V.6-14, Analysis User's Manual, Dassault Systèmes Simulia, Providence, RI, U.S.A.

Ansola, R., Canales, J., Tarrago, J.A. and Rasmussen, J. (2002), "An integrated approach for shape and topology optimization of shell structures", *Comput. Struct.*, **50**(5), 449-548. https://doi.org/10.1016/S0045-7949(02)00019-6.

ATC24 (1992), Guidelines for cyclic seismic testing of components of steel structures for buildings, Applied Technology Council, Redwood City, CA, U.S.A.

Bagherinejad, M.H. and Haghollahi, A. (2018), "Topology optimization of steel plate shear walls in the moment frames", *Steel Compos. Struct.,* **29**(6), 767-779. https://doi.org/10.12989/scs.2018.29.6.771.

Bendsøe, M. and Sigmund, O. (2003), *Topology Optimization: Theory, Methods, and Applications*, Springer-Verlag Berlin Heidelberg, New York, NY, U.S.A.

Bendsøe, M.P. (1989), "Optimal shape design as a material distribution problem", *Struct. Optim.*, **1**(4), 193-202. https://doi.org/10.1007/BF01650949.

Berman, J.W. and Bruneau, M. (2005), "Experimental investigation of light-gauge steel plate shear walls", *J. Struct. Eng.*, **131**(2), 259-267. https://doi.org/10.1061/(ASCE)0733-9445(2005)131:2(259).

Bhowmick, A.K., Grondin, G.Y. and Driver, R.G. (2014), "Nonlinear seismic analysis of perforated steel plate shear walls", *J. Constr. Steel Res.*, **94**, 103-113. https://doi.org/10.1016/j.jcsr.2013.11.006.

Buhl, T., Pedersen, C.B.W. and Sigmund, O. (2000), "Stiffness design of geometrically nonlinear structures using topology optimization", *Struct. Multidiscip. Optim.*, **19**(2), 93-104. https://doi.org/10.1007/s001580050089.

Chan, R., Albermani, F. and Kitipornchai, S. (2011), "Stiffness and strength of perforated steel plate shear wall", *Proced. Eng.*, **14**, 675-679. https://doi.org/10.1016/j.proeng.2011.07.086.

Dang, H., Lee, D. and Lee, K. (2017), "Single and multi-material topology optimization of CFRP composites to retrofit beam-column connection", *Comput. Concr.*, **19**(4), 405-411. https://doi.org/10.12989/cac.2017.19.4.405.

Dehghani, M., Mashayekhi, M. and Salajegheh, E. (2016), "Topology optimization of double-and triple-layer grids using a hybrid methodology", *Eng. Optim.*, **48**(8), 1333-1349. https://doi.org/10.1080/0305215X.2015.1105968.

Egorova, N. (2013), "Experimental study of ring-shaped steel plate shear walls", M.Sc. Dissertation, Virginia Polytechnic Institute and State University, Blacksburg, VA, U.S.A.

Egorova, N., Eatherton, M.R. and Maurya, A. (2014), "Experimental study of ring-shaped steel plate shear walls", *J. Constr. Steel Res.*, 103, 179-189. https://doi.org/10.1016/j.jcsr.2014.09.002.

Elgaaly, M. (1998), "Thin steel plate shear walls behavior and analysis", *Thin-Walled Struct.*, **32**(1), 151-180. https://doi.org/10.1016/S0263-8231(98)00031-7.

Formisano, A., Lombardi, L. and Mazzolani, F.M. (2016), "Perforated metal shear panels as bracing devices of seismic-resistant structures", *J. Constr. Steel Res.*, **126**, 37-49. https://doi.org/10.1016/j.jcsr.2016.07.006.

Gholizadeh, S. and Barati, H. (2014), "Topology optimization of nonlinear single layer domes by a new metaheuristic", *Steel Compos. Struct.,* **16**(6), 681-701. https://doi.org/10.12989/scs.2014.16.6.681.

Hassani, B. and Hinton, E. (1999), *Homogenization and structural topology optimization*, Springer-Verlag, London, United Kingdom.

Huang, X. and Xie, Y. (2010), "Evolutionary topology optimization of geometrically and materially nonlinear structures under prescribed", *Struct. Eng. Mech.*, **34**(5), 581-595. https://doi.org/10.12989/sem.2010.34.5.581.

Jansseune, A. and Corte, W.D. (2017), "The influence of convoy loading on the optimized topology of railway bridges", *Struct. Eng. Mech.*, **64**(1), 45-58. https://doi.org/10.12989/sem.2017.64.1.045.

Jung, D. and Gea, H.C. (2004), "Topology optimization of nonlinear structures", *Finite Elem. Anal. Des.*, **40**(11), 3443-3459. https://doi.org/10.1016/j.finel.2003.08.011.

Kabus, S. and Pedersen, C.B.W. (2012), "Optimal Bearing Housing Designing Using Topology Optimization", *J. Tribol.*, **134**(2), 1-9. https://doi.org/10.1115/1.4005951.

Kaveh, A., Hassani, B., Shojaee, S. and Tavakkoli, S.M. (2008), "Structural topology optimization using ant colony methodology", *Eng. Struct.*, **30**(9), 2559-2565. https://doi.org/10.1016/j.engstruct.2008.02.012.

Khatibinia, M. and Khosravi, S. (2014), "A hybrid approach based on an improved gravitational search algorithm and orthogonal crossover for optimal shape design of concrete gravity dams", *Appl. Soft. Comput.*, **16**, 223-233. https://doi.org/10.1016/j.asoc.2013.12.008.

Khatibinia, M., Roodsarabi, M. and Barati, M. (2018), "Topology optimization of plane structures using binary level set method and isogeometric analysis", *Int. J. Optim. Civil Eng.*, **8**(2), 209-226. http://ijoce.iust.ac.ir/article-1-341-en.html.

Kiani, J. and Tsavdaridis, K. (2018), "The Effect of Geometric Nonlinearity on the Seismic Performance of Steel Plate Shear Wall (SPSW) Systems", *Iranian J. Struct. Eng.*, **4**(2).

Kutyłowski, R. and Rasiak, B. (2014), "Application of topology optimization to bridge girder design", *Struct. Eng. Mech.*, **51**(1), 39-66. https://doi.org/10.12989/sem.2014.51.1.039.

Lee, E.H. and Park, J. (2001), "Structural design using topology and shape optimization", *Struct. Eng. Mech.*, **38**(4), 517-527. https://doi.org/10.12989/sem.2011.38.4.517.

Liu, A., X.Huang, C.Huang, G, S., Yan, X. and Li, G. (2017), "Topological design of structures under dynamic periodic loads", *Eng. Struct.*, **142**, 128-136. https://doi.org/10.1016/j.engstruct.2017.03.067.

Long, C.S., Loveday, P.W. and Groenwold, A.A. (2009), "Effects of finite element formulation on optimal plate and shell structural topologies", *Finite Elem. Anal. Des.*, **45**(11), 817-825. https://doi.org/10.1016/j.finel.2009.06.027.

Lu, X., Xu, J., Zhang, H. and Wei, P. (2017), "Topology optimization of the photovoltaic panel connector in high-rise buildings", *Struct. Eng. Mech.*, **62**(4), 465-475. https://doi.org/10.12989/sem.2017.62.4.465.

Mashayekhi, M., Salajegheh, E. and Dehghani, M. (2016), "Topology optimization of double and triple layer grid structures using a modified gravitational harmony search algorithm with efficient member grouping strategy", *Comput. Struct.*, **172**, 40-58. https://doi.org/10.1016/j.compstruc.2016.05.008.

Matteis, G.D., Sarracco, G. and Brando, G. (2016), "Experimental tests and optimization rules for steel perforated shear panels", *J. Constr. Steel Res.*, **123**, 41-52. https://doi.org/10.1016/j.jcsr.2016.04.025.

Maurya, A. (2012), "Computational simulation and analytical development of buckling resistant steel plate shear wall (br-spsw)", M.Sc. Dissertation, Virginia Polytechnic Institute and State University Blacksburg, VA, U.S.A. http://hdl.handle.net/10919/34466.

Maurya, A., Egorova, N. and Eatherton, M.R. (2013), "Development of ring-shaped steel plate shear walls", *Proceedings of the 2013 ASCE Structures Congress*, Pittsburgh, May.

Maute, K., Schwarz, S. and Ramm, E. (1998), "Adaptive topology optimization of elastoplastic structures", *Struct. Optim.*, **15**(2), 81-91. https://doi.org/10.1007/BF01278493.

Roberts, T.M. and Ghomi, S.S. (1998), "Hysteretic characteristics of unstiffened plate shear panels", *Thin-Walled Struct.*, **12**(2), 145-162. https://doi.org/10.1016/0263-8231(91)90061-M.

Roodsarabi, M., Khatibinia, M. and Sarafrazi, S. (2016), "Isogeometric topology optimization of structures using level set method incorporating sensitivity analysis", *Int. J. Optim. Civil Eng.*, **6**(3), 405-422. http://ijoce.iust.ac.ir/article-1-259-en.html.

Roodsarabi, M., Khatibinia, M. and Sarafrazi, S.R. (2016), "Hybrid of topological derivative-based level set method and isogeometric analysis for structural topology optimization", *Steel Compos. Struct.,* **21**(6), 1389-1410. http://dx.doi.org/10.12989/scs.2016.21.6.1389.

Seyedpoor, S. and Gholizadeh, S. (2008), "Optimum shape design of arch dams by a combination of simultaneous perturbation stochastic approximation and genetic algorithm methods", *Adv. Struct. Eng.*, **11**(5), 501-510. https://doi.org/10.1260%2F136943308786412069.

Shekastehband, B., Azaraxsh, A.A. and Showkati, H. (2017), "Hysteretic behavior of perforated steel plate shear walls with beam-only connected infill plates", *Steel Compos. Struct.,* **25**(4), 505-521. https://doi.org/10.12989/scs.2017.25.4.505.

Søndergaard, M.B. and Pedersen, C.B.W. (2014), "Applied topology optimization of vibro-acoustic hearing instrument models", *J. Sound Vib.*, **333**(3), 683-692. https://doi.org/10.1016/j.jsv.2013.09.029.

Svanberg, K. (1987), "The method of moving asymptotes - A new method for structural optimization", *Int. J. Numer. Meth. Eng.*, **24**(2), 359-373. https://doi.org/10.1002/nme.1620240207.

Tang, J., Xie, Y.M. and Felicetti, P. (2014), "Conceptual design of buildings subjected to wind load by using topology optimization", *Wind Struct.*, **18**(1), 021-035. https://doi.org/10.12989/was.2014.18.1.021.

Tenek, L.H. and Hagiwara, I. (1994), "Optimal rectangular plate and shallow shell topologies using thickness distribution or homogenization", *Comput. Meth. Appl. Mech. Eng.*, **115**(1), 111-124. https://doi.org/10.1016/0045-7825(94)90190-2.

TOSCA (2013), V.8.0, Tosca Structure Documentation, Dassault Systèmes Company, Karlsruhe, Baden-Württemberg, Germany.

Tsavdaridis, K.D., Kingman, J.J. and Toropov, V.V. (2015), "Application of structural topology optimisation to perforated steel beams", *Comput. Struct.*, **158**, 108-123. https://doi.org/10.1016/j.compstruc.2015.05.004.

Valizadeh, H., Sheidaii, M. and Showkati, H. (2012), "Experimental investigation on cyclic behavior of perforated steel plate shear walls", *J. Constr. Steel Res.*, **70**, 308-316. https://doi.org/10.1016/j.jcsr.2011.09.016.

Vatansever, C. and Yardimci, N. (2011), "Experimental investigation of thin steel plate shear walls with different infill-to-boundary frame connections", *Steel Compos. Struct.,* **11**(3), 251-271. https://doi.org/10.12989/scs.2011.11.3.251.

Vian, D., Bruneau, M., Tsai, K.C. and Lin, Y.C. (2009), "Special perforated steel plate shear walls with reduced beam section anchor beams. I: Experimental investigation", *J. Struct. Eng.*, **135**(3), 211-220. https://doi.org/10.1061/(ASCE)0733-9445(2009)135:3(211).

Wang, M., Yang, W., Shi, Y. and Xu, J. (2015), "Seismic behaviors of steel plate shear wall structures with construction details and materials", *J. Constr. Steel Res.*, **107**, 194-210. https://doi.org/10.1016/j.jcsr.2015.01.007.

Ye, H.L., Wang, W.W., Chen, N. and Sui, Y.K. (2016), "Plate/shell topological optimization subjected to linear buckling constraints by adopting composite exponential filtering function", *Acta Mech. Sin.*, **32**(4), 649-658. https://doi.org/10.1007/s10409-015-0531-5.

Yi, J., Rong, J., Zeng, T. and Huang, X. (2013), "A topology optimization method of multiple load cases and constraints based on element independent nodal density", *Struct. Eng. Mech.*, **45**(6), 759-777. https://doi.org/10.12989/sem.2013.45.6.759.

Yuge, K. and Kikuchi, N. (1995), "Optimization of a frame structure subjected to a plastic deformation", *Struct. Optim.*, **10**(3), 197-208. https://doi.org/10.1007/BF01742592.

Zhao, X., Liu, Y., Hua, L. and Mao, H. (2016), "Finite element analysis and topology optimization of a 12000KN fine blanking press frame", *Struct. Multidiscip. Optim.*, **54**(2), 375-389. https://doi.org/10.1007/s00158-016-1407-4.

Zhou, K. (2016), "Topology optimization of bracing systems using a truss-like material model", *Struct. Eng. Mech.*, **58**(2), 231-242. https://doi.org/10.12989/sem.2016.58.2.231.

CC